

KRISTJAN KALAM

Magnetic, electric and structural properties
of atomic layer deposited zirconia-based
nanolaminates and mixtures



KRISTJAN KALAM

Magnetic, electric and structural properties
of atomic layer deposited zirconia-based
nanolaminates and mixtures



The study was carried out at Institute of Physics, University of Tartu, Estonia.

The Dissertation was admitted on May 20, 2020 in partial fulfillment of the requirements for the degree of Doctor of Philosophy in Material Science and allowed for defense by Scientific Council on Material Science of the Faculty of Science and Technology, University of Tartu.

Supervisors: Aile Tamm (PhD), senior research fellow, Institute of Physics, University of Tartu, Tartu, Estonia.

Kaupo Kukli (PhD), research professor, Institute of Physics, University of Tartu, Tartu, Estonia.

Aarne Kasikov (PhD), researcher, Institute of Physics, University of Tartu, Tartu, Estonia.

Opponents: Robert Zierold (PhD), senior scientist, University of Hamburg, Hamburg, Germany.

Ivo Heinmaa (PhD), senior research fellow, National Institute Of Chemical Physics And Biophysics, Tallinn, Estonia.

Commencement: August 18, 2020 at the University of Tartu, Tartu, Estonia

This work has been partially supported by the European Regional Development Fund project “Emerging orders in quantum and nanomaterials” (TK134), Estonian Academy of Sciences (SLTFYPROF), Estonian Research Agency (IUT2-24 and PRG4) and Graduate School of Functional materials and technologies receiving funding from the European Regional Development Fund in University of Tartu, Estonia.



European Union
European Regional
Development Fund



Investing
in your future

ISSN 2228-0928

ISBN 978-9949-03-412-3 (print)

ISBN 978-9949-03-413-0 (pdf)

Copyright: Kristjan Kalam, 2020

University of Tartu Press

www.tyk.ee

TABLE OF CONTENTS

LIST OF ORIGINAL PUBLICATIONS AND AUTHOR'S CONTRIBUTIONS	6
LIST OF ABBREVIATIONS	8
THE CLAIM OF THE THESIS	9
INTRODUCTION	10
FERROMAGNETISM AND FERROELECTRICITY	12
ATOMIC LAYER DEPOSITION	14
EXPERIMENTAL METHODS	16
Spectroscopic Ellipsometry	16
X-Ray Diffraction.....	17
X-Ray Fluorescence Spectroscopy	18
Scanning Electron Microscopy	18
Magnetometry.....	19
Electrical Measurements.....	20
RESULTS AND DISCUSSION	22
Film Growth and Composition	22
Growth Per Cycle	22
Composition	24
Film Structure	25
Electrical Polarization.....	27
Resistive Switching Behavior.....	29
Ferromagnetic Properties.....	30
CONCLUSION	32
SUMMARY IN ESTONIAN	34
ACKNOWLEDGEMENTS	36
REFERENCES.....	37
PUBLICATIONS	43
CURRICULUM VITAE	91
ELULOOKIRJELDUS.....	92

LIST OF ORIGINAL PUBLICATIONS AND AUTHOR'S CONTRIBUTIONS

The present thesis is based on following original publications, referred in text with roman numerals I–V:

- I. **Kalam, K.**, Seemen, H., Ritslaid, P., Rähn, M., Tamm, A., Kukli, K., Kasikov, A., Link, J., Stern, R., Dueñas, S. and Castán, H., 2018. Atomic layer deposition and properties of ZrO_2/Fe_2O_3 thin films. *Beilstein Journal of Nanotechnology*, 9(1), pp.119–128.
<http://doi.org/10.3762/bjnano.9.14>
In this article the author's part was planning the experiments and their fulfilment, preparation of the samples via atomic layer deposition, and characterization using spectroscopic ellipsometry and X-ray diffraction. Additionally, the author gathered the experimental data, analysed, and formulated it into a written scientific paper.
- II. **Kalam, K.**, Seemen, H., Mikkor, M., Ritslaid, P., Stern, R., Dueñas, S., Castán, H., Tamm, A. and Kukli, K., 2018. Electric and Magnetic Properties of Atomic Layer Deposited ZrO_2-HfO_2 Thin Films. *ECS Journal of Solid State Science and Technology*, 7(9), pp. N117–N122.
<http://doi.org/10.1149/2.0041809jss>
In this article the author's part was planning the experiments and their fulfilment, preparation of the samples via atomic layer deposition, and characterization using spectroscopic ellipsometry and X-ray diffraction. Additionally, the author gathered the experimental data, analysed, and formulated it into a written scientific paper.
- III. **Kalam, K.**, Seemen, H., Mikkor, M., Jõgiaas, T., Ritslaid, P., Tamm, A., Kukli, K., Kasikov, A., Link, J., Stern, R. and Dueñas, S., 2019. Electrical and magnetic properties of atomic layer deposited cobalt oxide and zirconium oxide nanolaminates. *Thin Solid Films*, 669, pp. 294–300.
<http://doi.org/10.1016/j.tsf.2018.11.008>
In this article the author's part was planning the experiments and their fulfilment, preparation of the samples via atomic layer deposition, and characterization using spectroscopic ellipsometry and X-ray diffraction. Additionally, the author gathered the experimental data, analysed, and formulated it into a written scientific paper.
- IV. Tamm, A., Joost, U., Mikkor, M., **Kalam, K.**, Mändar, H., Seemen, H., Link, J., Stern, R., Castán, H., Dueñas, S. and Kukli, K., 2017. Properties of Zirconium Oxide and Cobalt Ferrite Layered Nanocomposite. *ECS Journal of Solid State Science and Technology*, 6(12), pp.P886–P892.
<http://doi.org/10.1149/2.0331712jss>

In this article the applicant prepared the zirconium oxide films for the nanocomposites using atomic layer deposition and investigated the structure of the composites with X-ray diffraction.

- V. Ossorio, O. G., Dueñas, S., Castán, H., Tamm, A., **Kalam, K.**, Seemen, H., and Kukli, K., 2018. Resistive Switching Properties of Atomic Layer Deposited ZrO₂-HfO₂ Thin Films. 2018 Spanish Conference on Electron Devices (CDE), pp. 1–4. IEEE.
<http://doi.org/10.1109/CDE.2018.8596925>
In this article the applicant deposited the samples and characterized them with X-ray diffraction and spectroscopic ellipsometry methods.

List of publications which are not included in this thesis:

- Kukli, Kaupo; Kemell, Marianna; Vehkamäki, Marko; Heikkilä, Mikko J.; Mizohata, Kenichiro; **Kalam, Kristjan**; Ritala, Mikko; Leskelä, Markku; Kundrata, Ivan; Fröhlich, Karol (2017). Atomic layer deposition and properties of mixed Ta₂O₅ and ZrO₂ films. *AIP Advances*, 7 (2), 025001.
<http://doi.org/10.1063/1.4975928>.
- Tamm, Aile; **Kalam, Kristjan**; Seemen, Helina; Kozlova, Jekaterina; Kukli, Kaupo; Aarik, Jaan; Link, Joosep; Stern, Raivo; Dueñas, Salvador and Castán, Helena (2017). Magnetic and Electrical Performance of Atomic Layer Deposited Iron Erbium Oxide Thin Films. *ACS Omega*, 2 (12), 8836–8842.
<http://doi.org/10.1021/acsomega.7b01394>.
- Kukli, Kaupo; Kemell, Marianna; Mizohata, Kenichiro; Vehkamäki, Marko; **Kalam, Kristjan**; Castán, Helena; Dueñas, Salvador; Link, Joosep; Stern, Raivo; Ritala, Mikko; Leskelä, Markku (2018). Atomic layer deposition of zirconium dioxide from zirconium tetraiodide and ozone. *ECS Journal of Solid State Science and Technology*, 7, P1–P8.
<http://doi.org/10.1149/2.0041802jss>.
- Seemen, Helina; Rähn, Mihkel; **Kalam, Kristjan**; Sajavaara, Timo; Dueñas, Salvador; Castán, Helena; Link, Joosep; Stern, Raivo; Kukli, Kaupo; Tamm, Aile (2018). Properties of Atomic Layer Deposited Nanolaminates of Zirconium and Cobalt Oxides. *ECS Journal of Solid State Science and Technology*, 7 (8), P402–P409.
<http://doi.org/10.1149/2.0191808jss>.

LIST OF ABBREVIATIONS

ALD – atomic layer deposition

GIXRD – grazing incidence X-ray diffraction

SE – spectroscopic ellipsometry

SEM – scanning electron microscope

VSM – vibrating sample magnetometer

XPS – X-ray photoelectron spectroscopy

XRD – X-ray diffraction

XRF – X-ray fluorescence

THE CLAIM OF THE THESIS

The author of the thesis claims that atomic layer deposition can be used to produce zirconia-based metal oxide thin films, which exhibit various electrical and magnetic properties, such as ferromagnetism, ferroelectricity and resistive switching. All these properties can feasibly be induced in oxide layers containing zirconium dioxide. Doping and multilayering of the films can induce the stabilization of metastable zirconia phases already in the as-deposited state enhancing the abovementioned properties.

Five original and published papers (denoted I–V) are presented to justify and discuss the claim.

INTRODUCTION

Multiferroism is traditionally regarded as a condition, where material exhibits more than one of the three ferroic properties: ferromagnetism, ferroelectricity, ferroelasticity [1]. Multiferroic materials, if produced in the nanoscale, could be used in novel memory materials, sensors, actuators and transducers [2–4]. Multiferroism seems to be an elusive property of a material, at least experimentally. It has also been theoretically studied, why so few of them exist [1]. Hill [1] concludes that transition metal d electrons, which are necessary for magnetism, drastically reduce ferroelectric properties. Therefore, ferromagnetism and ferroelectricity are somewhat contradictory properties. Despite these restrictive conditions, multiferroism is possible and even realized [1]. To the author’s knowledge, such a material, which would polarize in both magnetic and electric fields, has not been realized in the form of very thin film and working at room temperature or higher. Both of these conditions are necessary prerequisites for a real-world application. The possibility of the existence of several multiferroic materials in thin film form exploitable in electronics has been reviewed and predicted [5–6].

Another phenomenon, which could also be used for data storage in a potential next generation non-volatile memory, is resistive switching [7]. Several mechanisms have been suggested to explain resistive switching behavior [8–11], but the origin is still controversial. Resistive switching has been proven to occur in thin films at room temperature, but work is going on to find materials, which would work at lower switching voltages and have a greater difference between different resistance states. Resistive switching is a mechanism, where applied voltage induces a current in the material, but at some voltage, specific to the sample, current suddenly increases – resistance has suddenly decreased – and decreasing voltage after that point leads the current to be reduced, but at higher values than during the initial increase, because of the decreased resistance of the material, this hysteretic behavior is called the “set” process. A similar process may be carried out backwards, in reverse polarity, to again increase the sample resistance to the previous level, this would be the “reset” [12–14]. The above mentioned effect arises from the formation of a conductive filament inside the sample. By applying a voltage to a sample, a conductive filament of defects starts to form inside the sample and once this filament reaches from one electrode to another, resistance of the sample drops sharply. By applying a voltage of reversed polarity and sufficient amplitude, the filament may be broken again and result in a sharp increase of resistance to the previous level [2, 15].

ZrO₂ was chosen as a host material, since it already is a known memory material used in applications, such as the capacitor dielectric in dynamic random access memory [16–17]. Relying on literature [18–21], the author hypothesized that it should be possible to fabricate zirconia, which would also be ferromagnetic and/or exhibit resistive switching properties. Since other researchers have found the orthorhombic phase of HfO₂ to be ferroelectric [22–23], and ZrO₂ can also

theoretically exist in the orthorhombic phase, it was also hypothesized that ferroelectric zirconia is possible. Also, suitable doping or multilayering of zirconia was proposed to alter the structure of the material and enhance the above-mentioned properties.

Stabilizing the metastable phases of ZrO_2 at room temperature has been widely investigated [24–26]. It has been shown that in fact the metastable phases are behind some of the applicable properties of zirconia. For example, the orientationally averaged static dielectric constants are 36.8, 46.6, and 19.7 for the cubic, tetragonal and monoclinic ZrO_2 phases, respectively [27]. Ferromagnetism has been positively related to the tetragonal phase content [18].

Choice of method for fabrication was predicated on the fact that ALD is the best suited technique for producing very thin films with good uniformity over a large area [28]. In the current work, a multiferroic is meant to be a material, which is ferromagnetic and ferroelectric simultaneously. Ferroelasticity has not been investigated.

All the samples were fabricated in the Laboratory of Thin Film Technology, Institute of Physics, University of Tartu. Various methods for investigating the structure of materials were applied in the Laboratory of Thin Film Technology. Magnetometers were exploited in the National Institute of Chemical Physics and Biophysics, Tallinn. Electric field measurements were carried out in the University of Valladolid, Spain.

Some samples in this work have shown good resistive switching characteristics, most of them have been ferromagnetic and some have shown properties characteristic to a ferroelectric material. Although in the case of ferroelectricity, all samples have shown a remanent polarization charge, but mostly leakage current and interfacial polarization have contributed to this and ferroelectricity has only been established to be present in a few cases. Ferroelectric effect may be present in many more samples, but in most cases, even if present, overwhelmed by interfacial polarization and thus, undetectable. Few samples showed both ferromagnetic properties and in the case of charge polarization, at least a contribution from the ferroelectric effect.

FERROMAGNETISM AND FERROELECTRICITY

When a magnetic field, \mathbf{H} , is applied to a material, the response of the material is called its magnetic induction, \mathbf{B} . The relationship between \mathbf{B} and \mathbf{H} is a property of the material: $\mathbf{B}=\mathbf{H}+4\pi\mathbf{M}$, where \mathbf{M} is the magnetization of the medium. Magnetization is defined as the magnetic moment per unit volume [29].

In 1928, Heisenberg [30] showed that there is a term of electrostatic origin – Coulomb repulsion – in the energy of interaction between neighboring atoms which tends to orient the electron spins parallel to each other. This term is called the exchange integral, and it does not have a classical analog. The exchange interaction is in fact a consequence of the Pauli exclusion principle [29]. This exchange energy is minimized if all the electrons have the same spin. Opposing the alignment of spins in metals, and therefore the exchange energy, is the increased band energy involved in transferring electrons from the lowest band states to band states of higher energy. Such a transfer is necessary to align spins, because one orbital can hold two electrons with opposite spins and this configuration is energetically preferred to having two electrons in different orbitals. Aligning spins means two electrons can no longer occupy the same orbital and has to be transferred to a higher energy state. This band energy cost prevents simple metals from being ferromagnetic. In the elemental ferromagnetic transition metals, Fe, Ni, and Co, the Fermi energy lies in a region of overlapping 3d and 4s bands. The large number of electrons near the Fermi level reduces the band energy required to reverse a spin, and the exchange effect dominates [29].

Ferromagnetic domains are small regions in ferromagnetic materials within which all the magnetic dipoles are aligned parallel to each other. The boundaries between adjacent domains in bulk ferromagnetic materials are called domain walls. The width of domain walls is determined by a balance between competing energy contributions. The common explanation of ferromagnetism is that the domains are oriented randomly and result in a non-magnetized material, when no external field has been applied. When the field is applied, the domain whose magnetization is closest to the field direction starts to grow at the expense of the other domains. The growth occurs by domain-wall motion. Eventually the applied field is sufficient to eliminate all domain walls from the sample, leaving a single domain, with its magnetization pointing along the easy axis oriented most closely to the external magnetic field. Further increase in magnetization can only occur by rotating the magnetic dipoles from the easy axis of magnetization into the direction of the applied field. As soon as the magnetic field is removed, the dipoles rotate back to their easy axis of magnetization, and the net magnetic moment along the field direction decreases. Since the dipole rotation part of the magnetization process did not involve domain-wall motion, it is entirely reversible. Next, the demagnetizing field in the sample initiates the growth of reverse magnetic domains which allow the sample to be partially demagnetized. However, the domain walls are unable to fully reverse their motion back to their original positions. This is because the demagnetization process is driven by the

demagnetizing field, rather than an applied external field, and the demagnetizing field is not strong enough to overcome the energy barriers encountered when the domain walls intersect crystal imperfections. As a result, the magnetization curve shows hysteresis, and some magnetization remains in the sample even when the field is removed completely, this is called the remanent magnetization, or remanence. The coercive field, or coercivity, is defined as the additional field, applied in the reverse direction, which is needed to reduce the magnetization to zero [29].

Above explanation holds for traditional transition metal magnetism. However, it appears that in the nanoscale, ferromagnetism can arise in unexpected places. Thin films of materials, which in bulk have neither magnetic moments nor magnetic order, may appear ferromagnetic well above room temperature [31]. This will be discussed in the results section.

Many properties of ferroelectric materials are analogous to those of ferromagnets, but with the electric polarization, \mathbf{P} , corresponding to the magnetization, \mathbf{M} ; the electric field, \mathbf{E} , corresponding to the magnetic field, \mathbf{H} ; and the electric displacement, \mathbf{D} , corresponding to the magnetic flux density, \mathbf{B} . For example, ferroelectric materials also have domains and show a hysteretic response of both polarization and electric displacement to an applied electric field. Even the name ferroelectric is derived from the similarities to ferromagnetism, although ferroelectric behavior has no intersection with elemental iron [1].

A ferroelectric is an insulating system with two or more discrete states of different nonzero electric polarization in zero applied electric field, referred to as spontaneous polarization. For a system to be considered ferroelectric, it must be possible to switch between these states with an applied electric field, which changes the relative energy of the states through the coupling of the field \mathbf{E} to the polarization \mathbf{P} : $-\mathbf{E} \cdot \mathbf{P}$. For a finite system, electric polarization is straightforwardly defined as the dipole moment divided by the system volume [32]. For a crystal system to have these stable or metastable states, it must be non-centrosymmetric [1]. Cohen and Krakauer [33] modelled two perovskite-structure compounds – PbTiO_3 and BaTiO_3 – and found that Ti 3d–O 2p hybridization is essential for stabilizing the ferroelectric distortion. Börscke *et al* [22] have shown ferroelectric behavior in the orthorhombic $\text{HfO}_2 \text{Pbc}2_1$ phase, a noncentrosymmetric crystal group, which, as Börscke claims, is rare for HfO_2 .

ATOMIC LAYER DEPOSITION

Atomic layer deposition (ALD) is a chemical vapor phase technique capable of producing thin films of a variety of materials. Based on sequential, self-limiting reactions, ALD offers very good uniformity on various three-dimensional structures, thickness control at the Ångstrom level, and tunable film composition. With these advantages, ALD has proven to be a powerful tool for many industrial and research applications [28].

Dimensions of electronics components keep getting smaller, structures more complicated, thus microelectronics has become nanoelectronics. ALD has demonstrated potential advantages over alternative deposition methods, such as chemical vapor deposition and various physical vapor deposition techniques, due to its uniformity and control over materials thickness and composition. These desirable characteristics originate from the cyclic, self-saturating nature of ALD processes [28].

Most ALD processes are based on binary reaction sequences where two surface reactions occur and deposit a binary compound film. Because there are only a finite number of surface sites, the reactions can only deposit a finite number of surface species. If each of the two surface reactions is self-limiting, then the two reactions may proceed in a sequential fashion to deposit a thin film with atomic level control [34]. The current work also employed binary reaction sequences, but solid solutions and nanolaminates were created, using two different binary reactions in a certain order to obtain a given structure of two different metal oxides in the same film.

The first scientific work that could be regarded as the starting point of ALD, was carried out in the Soviet Union during 1960s. Results were published under the name of molecular layering in 1970 and 1974 [35–37]. Most likely due to the deposition rate deemed too slow, no practical applications emerged from these works. ALD was introduced as atomic layer epitaxy by Suntola and Antson in 1977, independently from their Soviet colleagues, depositing ZnS for flat panel displays [38] and this can be considered as the start of practical applications for ALD. More processes with different chemistries were studied and many materials were deposited non-epitaxially, so the more general name of atomic layer deposition became used [34, 39]

Depositing a binary compound, for example ZrO_2 , which is shown on figure 1, is managed in the following way:

Firstly, a pulse of metal precursor is introduced to the reaction chamber and a finite amount of it stays on nucleation sites of the substrate. Since no more of the precursor can adsorb on the substrate from the gaseous phase, increasing the pulse duration at this point would be useless. Secondly, a purge of inert gas is pumped into the reaction chamber, in order to remove the metal precursor, which is not adsorbed on the substrate, and this “leftover” precursor is pumped out of the reaction chamber. This is necessary for the next step, which is to introduce an oxygen source into the chamber. Since the purge has removed the metal precursor

not on the substrate, no reaction in the gas phase can occur, which is the main thickness control mechanism in ALD. Oxygen precursor reacts with the metal precursor on the substrate to form a metal oxide and the byproducts of the reaction are again purged out by an inert gas pulse following also the oxygen precursor pulse. Such four steps form a complete ALD cycle [34]. For an example of precursors and pulse times, in the current work, to deposit ZrO_2 , one of the used schemes was 4–4–2–8 s for the sequence of ZrCl_4 pulse–purge– H_2O pulse–purge.

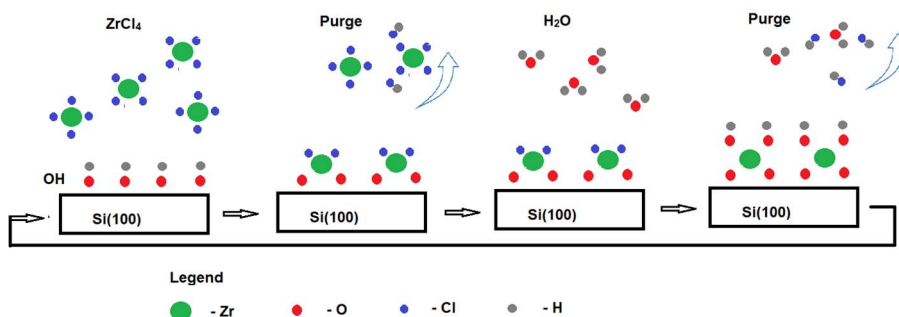


Figure 1. An illustration of ALD process for fabricating a ZrO_2 thin film. Color code of elements is given in the legend under the figure. Atomic radii on image are not to scale with real measured atomic radii of respective atoms.

Surface chemistry, nucleation and modelling the formation of ZrO_2 in ALD process is thoroughly investigated by other authors [40–42].

The rate of deposition in the case of ALD is not measured as film thickness being a function of time, but rather film thickness as a function of the amount of deposition cycles [28]. This is because of the self-limiting nature of ALD cycles. If the precursor pulse saturates the reaction chamber, then it does not matter how long the pulse is after saturation, growth is halted. Therefore, measuring growth as a function of time can be misleading and is not applied in the case of ALD.

In the current work, compounds consisting of two different metal oxides were mainly studied, either in the form of mixtures or nanolaminates. Throughout the text, the term cycle ratio is used to describe, how the compound was deposited. For example, a $\text{ZrO}_2:\text{Fe}_2\text{O}_3$ film, being deposited with a cycle ratio 5:5, means that firstly, 5 ALD cycles of ZrO_2 was deposited, then 5 ALD cycles of Fe_2O_3 was deposited on top of ZrO_2 and this scheme was repeated a certain amount of times.

EXPERIMENTAL METHODS

Spectroscopic Ellipsometry

Ellipsometry is an optical measurement technique, which exploits the reflection (or transmission) of light from the sample under study. The key concept of ellipsometry is the change in polarization of light that occurs, when light is reflected (or transmitted) from an object. The term ellipsometry stems from the fact that the polarization of light is generally elliptical after reflection. The ellipsometer measures two physical quantities: the ratio of electric field amplitudes, $\tan\Psi$, and the phase shift between s- and p-polarized light waves, Δ , which are defined by the complex reflection coefficients of s- and p-polarized waves, r_s and r_p , respectively:

$$\tan\Psi e^{i\Delta} \equiv \frac{r_p}{r_s}.$$

In spectroscopic ellipsometry (SE), these quantities are measured as a function of the incident light energy [43].

Presuming Ψ and Δ to be determined only by the reflection on the boundary between ambient air and the sample, Ψ and Δ can be related to the refractive indexes of ambient surroundings and the sample, and the angle of incidence, via Fresnel equations. This method is only applicable for a semi-infinite substrate. For a thin film on a substrate, a simple analytical equation cannot be derived but some kind of a dispersion model must be assumed and used for modelling [43].

The classical model for dispersion, derived from Newton's II Law, is the Lorentz model, which relates the complex dielectric constant of a material to the incident light wavelength. Simplification of the Lorentz model, where the imaginary part of complex refractive index is assumed to be zero, is the Sellmeier model. Expanding the function in Sellmeier model to a power series, the common Cauchy model is derived:

$$n = A + \frac{B}{\lambda^2} + \frac{C}{\lambda^4} + \dots$$

Experiments have shown that partly amorphous films and oxides are often not very well modelled by the Cauchy model, and thus the Tauc-Lorentz model has been proposed, using the abovementioned classical models and some empirical observations. For example, the fact that the imaginary part of the complex refractive index behaves differently for partly amorphous materials than the Lorentz model would suggest [43, 44].

All dispersion models are essentially the functions that relate the dielectric constant to the incident light wavelength. Some model must be assumed to

describe the measured data and from a successful modelling, some material parameters, such as the thickness and refractive index, can be extracted as well.

Range of incident light energies for measurement was 1.7–6.5 eV. Angle of incidence is chosen sufficient to ensure the maximum sensitivity of the measurements, depending on the sample being measured. In the present work this angle was usually 70°. Ellipsometry enables to calculate many physical quantities from the obtained parameters, but the main target, also in the current work, was to obtain the thicknesses and refractive indexes of the samples. Spectroscopic ellipsometer, model GES5-E, was thus used for the measurements of the films thicknesses and refractive indexes.

X-Ray Diffraction

When an X-ray photon falls on an atom, it may be absorbed or scattered. Scattering may be coherent or incoherent. The X-ray diffraction (XRD) technique uses the coherent scattering of X-rays by the sample under study. It was discovered in 1912 by Max von Laue that the crystal lattice of a material can act as a diffraction grating for the incident X-rays. Due to constructive interference, the crystal lattice produces a characteristic set of maxima at various scattering angles for the X-rays. Every crystal lattice phase composition has a unique set of such maxima and therefore, the phase composition can thus be determined [45].

The most common XRD technique is the powder diffraction, where the sample is ground to a very fine powder. In the case of very thin films, such as in the current work, the films must be on some kind of a substrate. Using similar incidence angles for thin films on substrates, as for powders, all the information obtained would be from the substrate and information from the film would be heavily overwhelmed by it. In order to measure thin films on substrates, the grazing incidence X-ray diffraction (GIXRD) has been developed.

The GIXRD method uses a very small angle of incidence. It is necessary to note here that the angle of incidence is measured differently from conventional optics. In the X-ray diffraction literature, angle of incidence is measured as an angle between the incident X-ray and the tangent of the sample surface. A very small, grazing, incidence beam with its geometry therefore means a very large angle between the incident X-ray and the surface normal vector. Such a measuring technique ensures that the X-rays do not penetrate the sample very deeply, but instead, most of the radiation is scattered by the very thin top layer of material. Therefore, the signal from the substrate will play a much less significant role in the diffraction pattern, compared to traditional incidence angles [46].

Since all the samples in the current work were very thin films, often only 5–20 nm, the GIXRD technique was employed to estimate the phase composition of the films. X-rays with a wavelength of 0.15406 nm were used, which is the Copper K_{α} energy. X-ray diffractometer SmartLab Rigaku was used for the measurements.

X-Ray Fluorescence Spectroscopy

Unlike XRD, X-ray fluorescence spectroscopy (XRF) makes use of the absorption of X-rays in the sample under study. When a material is subjected to X-rays, this radiation may be absorbed by its component atoms. If the absorbed radiation ionizes the atom by exciting one or more electrons out of the inner shell of the atom, electrons from higher orbitals will fill this gap and thus release energy in the form of photons. These released photons have the energy corresponding to the energy differences between orbitals and, therefore, characteristic of the atoms present in the sample. If this re-emission has a different energy than the incident X-rays, then the phenomenon is called fluorescence [47].

Since the XRF radiation is characteristic of atoms present in the sample, bombarding the sample with X-rays and registering the resulting fluorescence gives us quantitative information about the atomic composition of the sample. It should be noted that the output of this characterization method is the mass amount of each atom in the sample, but it does not provide information about the chemical bonds between these atoms. Such information can directly be obtained by X-ray photoelectron spectroscopy, for example, but this leaves the scope of this work.

Composition of all samples in this work was determined by using the XRF method and the crystalline chemical compounds under investigation were determined by using GIXRD in addition to XRF. The general idea was to use atomic masses of elements and amounts measured by XRF. For example, since the mass of zirconium atom is 5.7 times higher than the mass of the oxygen atom, then measuring the mass of zirconium to be around $5.7/2=2.85$ times higher than that of oxygen, gives good reason to believe that the compound in the sample is ZrO_2 . Measuring the crystallinity of the sample by GIXRD and finding the best match to be a known phase of ZrO_2 , for example tetragonal, in the author's view, determines the sample to contain tetragonal ZrO_2 convincingly, also amorphous ZrO_2 may be present, which can not be determined by GIXRD studies. Residual chlorine and carbon contents were measured as well, if the precursors contained either of them. Spectrometer Rigaku ZSX 400 and program ZSX Version 5.55 was used in this work.

Scanning Electron Microscopy

The scanning electron microscope (SEM), as the name suggests, is a device to enlarge small objects otherwise invisible to human sight. These images are obtained by scanning a high-energy electron beam on the sample surface. Because electrons have a much smaller wavelength, the resolution of the SEM is much larger than that of the regular optical microscope. SEM is not only able to produce images, but, as the interaction between the electron beam and the sample produces X-rays characteristic of the sample material, the composition of the sample can also be determined. [48]

In the current work, the composition determination was done with XRF, not the SEM, but another useful feature of the SEM was used for selected samples, the transmission electron microscope (TEM). Using higher electron beam energies, the electron microscope can be made to operate in the transmission mode, registering electrons transmitted through the sample. SEM using a Dual Beam equipment FEI Helios NanoLab 600 was used to obtain images visualizing the surface of the samples. In some cases, in this work, high resolution images of the sample cross-section were desired and in such cases, a thin lamella was cut from the sample and the cross-section was subjected to a transmission electron beam to form the image.

Magnetometry

A very general description of magnetic measurement is that a sample produces a force, flux or indirect signal, which is sensed by a detector and results in an output which is usually an electric signal. The detector defines the principle employed and the response obtained. A sample produces a distortion in the field affecting the flux distribution. A flux detector senses such a change. The sensor is usually a coil but can also include a variety of indirect sensors. A specimen in a non-uniform field experiences a force, detected by a force transducer. Methods which use force or flux detection are classified as direct techniques, and all the others are indirect techniques. [49]

All the magnetometry measurements in this work have been performed using a vibrating sample magnetometer (VSM). The output of this method for the current work was measuring the magnetization of the sample for a wide range (-5000 Oe to 5000 Oe) of magnetic field strength at room temperature. Sweeping the magnetic field from positive to negative and vice versa, reveals if the magnetization values follow a different curve, depending on whether the magnetic field is increasing or decreasing at the given moment. If so, this produces a hysteresis, which implies some form of ferromagnetism, which was the phenomenon of interest in this work. VSM option of the Physical Property Measurement System 14T Quantum Design was used in this work, by scanning the magnetic field from -5000 Oe to 5000 Oe parallel to the film surface at room temperature.

The VSM was invented at MIT Lincoln Laboratory by Simon Foner, who introduced it to the general public in 1959. In this method the sample is vibrated at small amplitude with a known frequency and phase in a uniform applied field. The field distortion produced by the sample varies in a sinusoidal manner, is detected by a registering coil, and is processed with conventional alternating current processing equipment. The induced voltage in the registering coil is proportional to the sample's magnetic moment, but does not depend on the strength of the applied magnetic field. The coils for registering the field distortion are generally attached to the magnet in order to avoid vibration of the coils with respect to the magnet [50].

There is no one-to-one correspondence between magnetization and external magnetic field in ferromagnetic materials, because of magnetic hysteresis, but a formula can be given to relate the magnetization m to the remanence B_r :

$$m = \frac{1}{\mu_0} B_r V,$$

where μ_0 is the permeability of vacuum and V is the volume of the sample. But the magnetization of the sample induces an electromotive force ϵ in the coils of the magnetometer, which is related to the magnetization m as follows:

$$\epsilon = \frac{3}{4\pi} \mu_0 m \omega g_I,$$

where ω is the angular frequency of sample oscillation, g_I is the instrument factor. The value of g_I is determined with calibration, measuring a sample with known magnetic moment [51].

Electrical Measurements

The Sawyer-Tower circuit is a measurement technique to record the hysteresis loop of a ferroelectric material. The original circuit, assembled by Sawyer and Tower in 1929 [52], was to measure the ferroelectricity of Rochelle salt. The heart of the circuit are two capacitors in series, one is the sample and the other is a capacitor with known parameters. Since the charge on the plates of series capacitors is equal, the polarization charge Q_x in the sample can be calculated by measuring the voltage on the known-value capacitor V_{sense} and multiplying the value with its capacitance C_{sense} [53]:

$$Q_x = Q_{sense} = C_{sense} V_{sense}$$

By sweeping the applied voltage on the circuit and registering the corresponding polarization charge values, a graph can be obtained, depicting the polarization charge depending on the applied voltage (or electric field). In the case of a ferroelectric material, a hysteresis loop appears in such a graph.

Measured charge in the circuit is a charge that is on the plates of a capacitor. However, when voltage is applied, the accumulating charge on the plates may not be only due to ferroelectric polarization. Another quite common reason is the leakage of the sample and defects near the electrodes, moving charges due to defects in the material drifting from electrode to the counterelectrode in an applied field and then getting trapped in defects near the electrodes, in the interface of electrode and functional layer. It is quite natural to assume the density of defects to be highest at the interface, because of the lattice mismatch of two materials. Such an effect was indeed also observed in this work and in fact, for many cases,

this interfacial polarization overwhelmed any ferroelectric effect that might have been present, the latter effects existence could therefore not be identified.

Electrical polarization measurements were recorded by Agilent DXO-X 3104 digital oscilloscope with a built-in wave generator. The Sawyer-Tower experiment was carried out by applying a periodic triangular-shaped stimulus and recording the voltage loops from the oscilloscope. Charge values were obtained from the sensed voltage across a known capacitance.

The phenomenon of resistive switching is a complicated one and the origin of it is still controversial [7]. However, the determination of this effect in a material is quite straightforward, it can be seen on a voltage-current curve if the voltage is swept from positive to negative values and vice versa.

Resistive switching measurements were carried out by means of a semiconductor analyzer Keithley 4200SCS, with samples put in a light-tight and electrically shielded box. The voltage was applied to the top electrode, leaving the bottom one grounded.

Films under study were deposited on substrates, where there was a titanium nitride layer on silicon, in order to avoid a parasitic capacitor forming between the functional layer and the substrate. Electrodes for conducting electrical measurements were made using the electron beam evaporation method. A layer of aluminum was evaporated on the backside of the substrate, Si(100). On top of the functional dielectric layer, metal electrodes with an area of 0.204 mm^2 were evaporated. This metal was either platinum or titanium, since these metals do not form a notable intermediate layer between the oxide and electrode, when coming to contact with each other.

RESULTS AND DISCUSSION

Film Growth and Composition

Growth Per Cycle

Growth per cycle depends mostly on the reaction chamber temperature and, plausibly, on the process chemistry, that is, precursors used for the reaction. Additionally, the film growth rate can be influenced by the structure and/or chemical inertness of the substrate surface. The films in this work were deposited mostly on Si(100) substrates, and, for electrical measurements, TiN substrates were also used. In some deposition experiments, three-dimensional (3D) silicon stacked structures were used, with an aspect ratio of 1:20, as substrates, to demonstrate conformal growth on non-planar surfaces.

ZrO₂ was deposited from zirconium tetrachloride, ZrCl₄, while the oxygen source was either water, H₂O, or ozone, O₃. Growth temperature was 300 °C in most of the depositions. ZrO₂ growth rate was measured for various substrate temperatures, using SE to measure thickness and divide it with the number of cycles. At 300 °C, the rate was 0.13 nm/cycle. At higher temperatures, 350 °C and 400 °C, the growth rate diminished to 0.10 and 0.12 nm/cycle, respectively, likely due to the decreasing density of active adsorption sites, i.e., OH-groups on the surface at higher temperatures. The growth rate, on the other hand, was dropped to 0.06 nm/cycle at the lowest temperature examined, i.e. at 250 °C, likely due to the proximity of thermal reaction threshold. Therefore 300 °C was chosen as the chamber temperature for the ZrO₂ growth experiments, to achieve the optimum deposition rate. It must be noted that these results were obtained for reference films with thicknesses 30–50 nm. When depositing very thin films, less than 15 nm, the deposition rate was slightly lower, because of the incubation period, which is a period of nonlinear growth at the beginning of the deposition. In the case of ZrO₂:Fe₂O₃ film growth, however, the chamber temperature was chosen to be 400 °C, instead of 300 °C, since Fe₂O₃ was deposited from ferrocene, Fe(C₅H₅)₂ and O₃, and these precursors have earlier provided relatively slow growth rate at 300 °C [54]. At 400 °C, Fe₂O₃ deposition rate was increased to 0.18 nm/cycle [I]. Therefore, one had to find a compromise between optimum temperatures for ZrO₂ and Fe₂O₃ deposition experiments in the present study. For depositing Co₃O₄ from Tris(2,4-pentanedionato)cobalt, Co(acac)₃, and O₃, it was found that the optimal deposition temperature for these precursors, at a pressure of about 220 Pa, was 300 °C, giving the deposition rate of 0.06 nm/cycle. Reducing the temperature to 250 °C resulted in a 50% lower deposition rate and raising the temperature to 350 °C resulted in a 60% lower deposition rate. At low temperatures, the lower rate was, again, likely due to approaching the reaction threshold. At high temperatures, the lower rate was quite possibly caused by the thermal decomposition of the precursor in the gas phase, before reaching the substrate surface. Therefore, it appeared not reasonable to work in the ALD

regime outside the temperature range of 250 – 350 °C, in the case of given process chemistry [III]. HfO₂ was deposited from hafnium tetrachloride, HfCl₄, and H₂O at 300 °C, analogously to its relative compound ZrO₂, and the growth rate of 0.10 nm/cycle was achieved [I].

Generally, deposition rates of binary oxides can be measured and are necessary to know when working with them, but they do not tell us anything definitively about what happens when two binary oxides are mixed together. One may only presume that a compound of two metal oxides might have a deposition rate lower than either metal oxides separately [55]. This is a result of a chemical compound growing most rapidly on itself and less rapidly on materials of foreign composition. From that argument, it logically follows that alternating different materials should most likely proceed with a lower deposition rate compared to processes with alternating layers of the same materials. For example, combining Fe₂O₃ films, which were previously mentioned to have a growth rate of 0.18 nm/cycle, and ZrO₂ films with a growth rate of 0.12 nm/cycle, produced films with growth rates of 0.11 and 0.09 nm/cycle in the cases of Fe₂O₃:ZrO₂ cycle ratios of 10:10 and 5:5, respectively [I].

When growing nanolaminates of ZrO₂ and Co₃O₄ [III], it was concluded that the deposition rate of ZrO₂ depended on whether it was grown on the Si(100) substrate or on a previously deposited Co₃O₄. Deposition rate of ZrO₂ on Si(100) in this work was found to be 0.10 nm/cycle, but on Co₂O₃ it was 0.14 nm/cycle, which was equal to the growth rate of undoped thicker ZrO₂ reference films [III]. Growth rate of ZrO₂ in the work III was higher than in the work I, because the deposition temperature was 300 °C in the former case and 400 °C in the latter case. In the case of chloride based ALD processes, including that of ZrO₂, the higher growth rate at lower substrate temperature was expected, as it has been observed in earlier studies [56].

In the case of mixing ZrO₂ and HfO₂ with various cycle ratios, it was observed that the lowest deposition rates occurred when the cycle ratio was 10:3, regardless of which oxide was deposited in majority. One cycle of an oxide material deposited between the thicker layers of a different, dominating oxide did not inhibit growth that much, probably because one cycle could not produce a continuous monolayer of a particular compound material, whereas three cycles may produce a continuous layer, which can make deposition of another constituent material on that previously deposited layer slower. Also, comparing materials growing on each other and on silicon substrate, zirconia appeared to grow equally fast on Si(100) and hafnia, but hafnia grew faster on Si(100), than on ZrO₂ [II].

The nucleation of every oxide is slower during the first few deposition cycles, and the content of metal deposited does not linearly correspond to the amount of cycles at the early stages of the growth. This phenomenon can be referred to as the incubation time. The nonlinearity of the thickness as a function of growth per cycle was also observed with HfO₂ [57] and ZrO₂ [58]. Since this incubation time varies in different materials, the result is that cycle ratio does not match the cation ratio in a compound of two metal oxides.

Deposition of Fe₂O₃ using Fe(C₅H₅)₂ and O₃, carried out at 400 °C, proceeded with the growth rate of 0.18 nm/cycle, which can be compared with the values obtained by Martinson *et al* [54], who found the deposition rate to be 0.14 nm/cycle for the same precursors, although at 200 °C. Martinson *et al* [54] achieved a relatively large deposition rate for such a low temperature, but at the cost of extremely long precursor pulses. In the present work, one Fe₂O₃ ALD cycle was carried out within 20 s, whereas in the work by Martinson *et al*, it was 340 s [54]. Deposition rate of ZrO₂ was around 0.12 nm/cycle in all experiments for 300 °C deposition temperature, which is again consistent with some earlier studies [59–60].

Composition

The zirconium oxide films grown in the present study could be characterized as zirconium dioxide, in terms of stoichiometry, and in the accuracy limits of spectrometric evaluation methods. The films were also markedly crystallized, and the GIXRD results support the observations on formation of dominantly dioxide phases, as will be described below. The same was valid for other oxides constituting the laminates or mixtures with ZrO₂, i.e. HfO₂ and Fe₂O₃. In regard with the mixture and laminate films, it is important to note about their composition that, although the ratio between the amounts of component oxide deposition cycles does not directly correspond to the cation ratio, these parameters were correlated. In the case of HfO₂:ZrO₂ films, the cycle ratios were varied as follows: 1:10, 3:10, 5:10, 10:10, 10:5, 10:3, 10:1. For the same films, hafnia content Hf/(Hf+Zr) was measured with XRF and the results are given in Table I.

Table I. HfO₂:ZrO₂ cycle ratios and cation ratios, calculated by cycle ratio, and measured with XRF.

HfO ₂ :ZrO ₂ cycle ratio	1:10	3:10	5:10	10:10	10:5	10:3	10:1
Hf/(Hf+Zr) based on cycle ratio	0.09	0.23	0.33	0.50	0.67	0.77	0.91
Hf/(Hf+Zr) measured	0.17	0.46	0.64	0.47	0.91	0.73	0.90
Film thickness, nm	17	10	14	20	18	14	22

Table I implies that HfO₂ grows faster, during the first 10 ALD cycles, than ZrO₂. This was concluded, since hafnia doped with zirconia systematically exhibited larger thickness values for the same cycle ratios and cycle amounts than zirconia doped with hafnia. Also, hafnia content was larger than cycle ratio would imply [II].

Similar results were obtained in the case of mixing ZrO₂ with Fe₂O₃, where the application of ZrO₂:Fe₂O₃ cycle ratio of 5:5 produced a Zr/Fe cation ratio of 0.16. This implies that the growth of ZrO₂ was much more retarded during the

first 5 ZrO₂ growth cycles compared to those of Fe₂O₃. When the amount of ZrO₂ deposition cycles were increased two times, making a cycle ratio of 10:5 for ZrO₂:Fe₂O₃, then the Zr/Fe cation ratio was increased over ten times, reaching 2.0 [I].

Since the used precursor for ZrO₂ was ZrCl₄, it could be assumed that some residual Cl was left in the films. This was seen with X-ray photoelectron spectroscopy (XPS) [IV] and measured by XRF to range between 0.3–0.5 wt%. In the case of Co(acac)₃ as a precursor for Co₃O₄, amount of carbon residue was measured with XRF to be 3.3–7.8 wt% [III].

Film Structure

Most films were at least partly crystalline in the as-deposited state, especially binary metal oxides. Co₃O₄ film was determined to have a cubic lattice ordering [III], HfO₂ and Fe₂O₃ possessed dominant monoclinic structure [I, II] and ZrO₂ appeared mostly as a mixture of cubic and tetragonal phases [I–IV]. However, small diffraction maximums indicated also the monoclinic phase of ZrO₂ apparent in the diffractograms, providing that the ZrO₂ films were not doped or multilayered with foreign metal oxides. If ZrO₂ was doped with a small amount of another metal oxide, the diffraction maximums characteristic of the monoclinic phase disappeared and the only crystalline ordering left was that characteristic of cubic and tetragonal polymorphs. Apparently, both doping ZrO₂ with a small amount of foreign material and depositing it in the form of films to rather low thicknesses (20–30 nm) contributed to the room-temperature stabilization of the metastable crystalline phases. For some mixtures or nanolaminates with ZrO₂, no diffraction maxima could be detected at all. This was somewhat expected, since mixing materials interferes the crystallization process by deforming lattices and the formation of lattice can easily become inhibited. After every 10 ALD cycles, for example, the growth of a materials lattice was halted and the sequence was continued by deposition of another, chemically distinct material constituting the periodical multilayers or nanocomposites using comparable amounts of ALD cycles for the next constituent. Figure 2 illustrates these observations, as it shows un-doped ZrO₂ to be mostly a mixture of cubic and tetragonal phases. Small diffraction maxima, which are unmistakably attributable to the monoclinic phase, are also visible. Doping ZrO₂ with HfO₂ made the –111 and 111 reflection peaks of the monoclinic phase disappear, but also overall crystallinity was decreased, obviously. Un-doped HfO₂ is clearly mostly monoclinic, revealing weak traces of cubic lattice, that is, a small “bump” above the noise level, where the diffraction maximum attributable to the reflection from cubic 111 plane should appear [II].

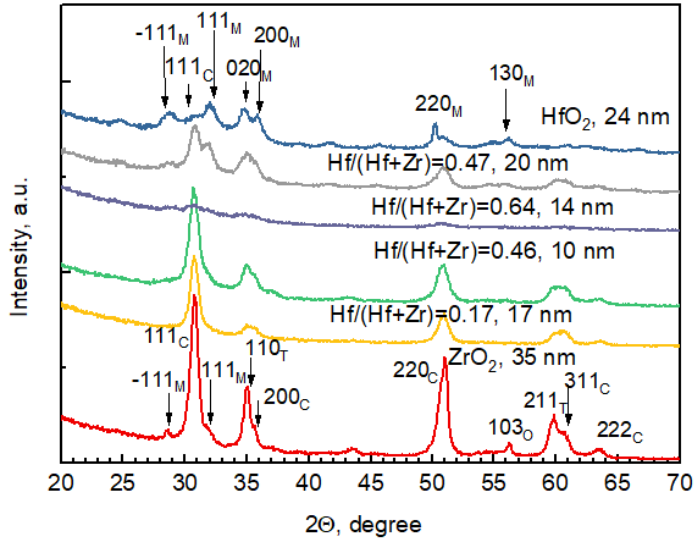


Figure 2. GIXRD patterns for un-doped ZrO_2 , HfO_2 and hafnia-doped zirconia. The composition and thicknesses of the films are indicated by the labels at the patterns. Miller indexes are attributed to corresponding monoclinic (M), cubic (C), tetragonal (T) and orthorhombic (O) phases [II].

In the case of un-doped ZrO_2 , which was deposited from ZrCl_4 and O_3 at $300\text{ }^\circ\text{C}$, the relative permittivity was measured to be 26. This is related to the crystal structure of the films as Zhao and Vanderbilt [27] have calculated that cubic, tetragonal and monoclinic ZrO_2 should possess average permittivity of 36.8, 46.6 and 19.7, respectively. Assuming that the un-doped ZrO_2 film was completely crystallized and consisted of only cubic and monoclinic phases, then this should lead to the conclusion that the phase composition of our film contained 63% of the monoclinic and 37% of cubic phase. Since the GIXRD analysis revealed mostly cubic and tetragonal phases actually present in the films, together with traces from monoclinic phase, we can assume that the film was not completely crystalline, but including amorphous regions in addition to those ordered up to clearly defined cubic and tetragonal crystal lattices [III].

Along with the ALD experiments on mixed layers, it became important to demonstrate, whether a process of depositing a mixture of two metal oxides could result in a conformal growth over a non-planar substrate surface. The substrate surface used was that of a stacked three-dimensional structure of silicon substrate with an aspect ratio of 1:20. Figure 3 represents a cross-sectional SEM image of such a sample. One can see, that the film has been deposited inside the stacked structure [I].

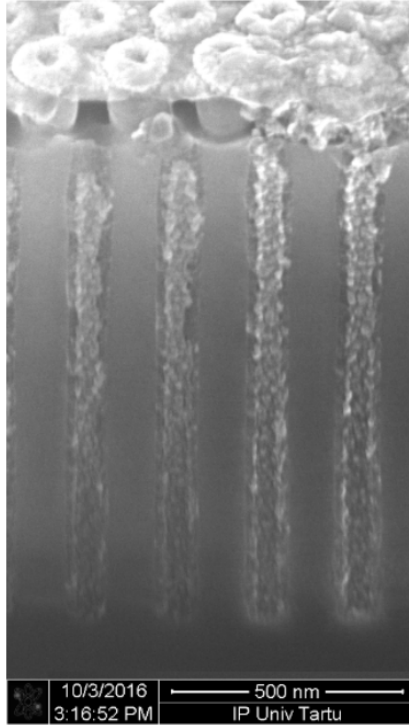


Figure 3. SEM image of a $\text{ZrO}_2/\text{Fe}_2\text{O}_3$ film grown in a 3D stacked structure [I].

Electrical Polarization

In the $\text{ZrO}_2:\text{HfO}_2$, $\text{ZrO}_2:\text{Fe}_2\text{O}_3$, $\text{ZrO}_2:\text{Co}_3\text{O}_4$ and $\text{ZrO}_2:\text{CoFe}_2\text{O}_4$ samples polarization charge hystereses were observed [I–IV]. No tendency to saturation was observed, though, in the charging along increasing external field strength for $\text{ZrO}_2:\text{Fe}_2\text{O}_3$, $\text{ZrO}_2:\text{Co}_3\text{O}_4$ and $\text{ZrO}_2:\text{CoFe}_2\text{O}_4$ samples [I, III–IV], which otherwise is a typical property of ferroelectric hysteresis. Instead, polarization charge just increased upon increasing the applied field and, when measuring the leakage currents of samples, it was observed that more leaking samples produced larger polarization charge loops in the Sawyer-Tower measurement. A typical example of such a loop is shown on figure 4 [I]. For this reason, specific “remanence” and “coercivity” values for these samples do not have too much quantitative value, because such loops can be recorded for various electric field and charge polarization values [I, III–IV]. For $\text{ZrO}_2:\text{HfO}_2$ samples, example of which is on figure 5, hysteresis loops resembled actual ferroelectrics, showing remanent polarization values around $30\text{--}90\text{ mC/cm}^2$ and coercive field values $1\text{--}2\text{ MV/cm}$. While coercive field values are similar to literature, polarization charge values exceed comparable literature results [23, 61] by three orders of magnitude, which implies still a large contribution from interfacial polarization [II].

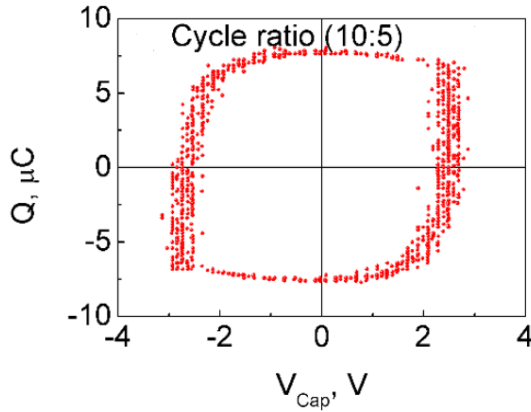


Figure 4. Polarization charge – applied voltage curve for a Pt/ZrO₂:Fe₂O₃/TiN/Ti/Si(100)/Al sample [I].

Similar loops to ZrO₂:Fe₂O₃ samples have been published in a number of works on other materials, reporting ferroelectric behavior. For example, ferroelectric hysteresis in LiNbO₃ [62–63], Bi₄Ti₃O₁₂ [64] and Pb(Zr,Ti)O_x [65] have been claimed, while providing similar measurements revealing curves analogous to those in Figure 4. The author of the present study recognizes that such loops, without visible saturation, cannot be claimed to illustrate ferroelectric behavior. This does not mean that ferroelectricity doesn't exist in such samples, but even if present, it is essentially overwhelmed by leakage current and, likely, interfacial polarization. The author's view on this matter coincides with that of Scott [66], who quite blatantly calls such figures bananas and urges authors not to publish such bananas with claims of ferroelectricity. One can propose, after observations on the ZrO₂:Fe₂O₃ samples that, even if the contribution from ferroelectricity is not to be completely eliminated, it cannot dominate such curves (Figure 4). Instead, this polarized charge in applied field is plausibly due to leakage currents in the samples. Similar “bananas” were observed also in [III] and [IV].

Curves actually resembling a hysteresis loop were observed in a work devoted to HfO₂:ZrO₂ films [II]. Loops that show saturation and have a concave region, such as those described by Martin *et al* [67] were shown [II]. Figure 5 shows a characteristic curve from HfO₂:ZrO₂ nanolaminate films [II], where tendency to saturation can be observed. In these samples, leakage has a marked role as well, since the polarization charge values are quite large, considerably larger than other reports on real ferroelectrics, that do not look like “bananas” [23, 61, 68]. The main difference in this case is the saturation of the charge values together with moderate remanent polarization charge and defined coercivity, which is a clear implication that ferroelectric behavior exists along with leakage current.

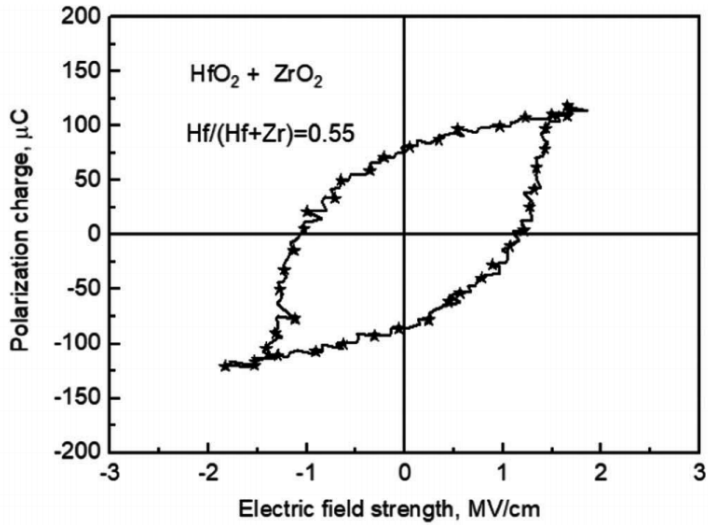


Figure 5. Electrical polarization-applied field loops measured from a nanolaminate film consisting of 10 nm thick HfO_2 and 8 nm thick ZrO_2 layers. Cation ratio 0.55 is also given on the figure [III].

Resistive Switching Behavior

The result of resistive switching is a memory effect, hysteretic behavior and a corresponding loop on the voltage-current curve, example of which is in Figure 6.

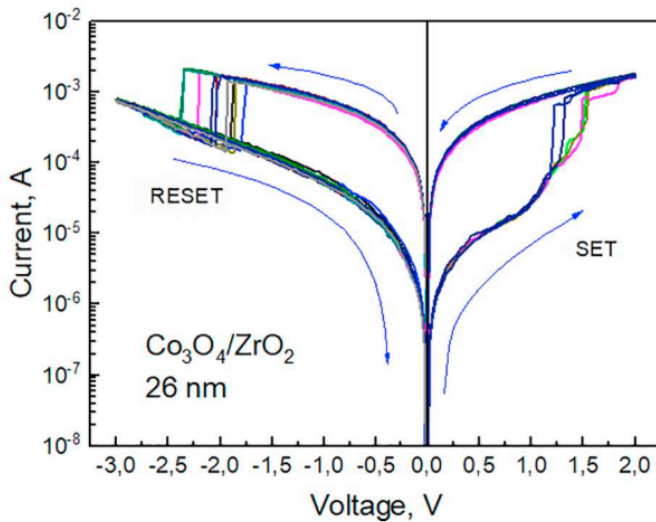


Figure 6. Resistive switching cycles for a $\text{Co}_3\text{O}_4/\text{ZrO}_2$ nanolaminate. The composition and thickness of the metal oxide layers are indicated by labels [III].

For the $\text{Co}_3\text{O}_4/\text{ZrO}_2$ sample on figure 6, the resistance ratio of the high and low resistance states was 35. For other films this ratio was 3–4. Resistance states were compared at a voltage of 0.5 V. For films with sharp well-defined switches between high and low resistance states, this switch occurred in the range of 1.5–3 V for various films [III]. For comparable films, a resistance ratio of an order of magnitude is adequate, but the switching voltage should be lower, compared to literature, a formidable switching voltage would be 1 V or less [17]. Switching voltage around 1 V was measured in the case of $\text{HfO}_2:\text{ZrO}_2$ films, although lower resistance ratio, 2–3, was observed for various samples [V]. $\text{ZrO}_2\text{--CoFe}_2\text{O}_4$ samples exhibited similar resistive switching characteristics to $\text{HfO}_2:\text{ZrO}_2$, but with higher switching voltages, 1.2 V for “set” and 2.2 V for “reset” [IV]. For all samples, we proposed the defects responsible in the formation of the filament are oxygen vacancies [III–V]. This is also the reason ferromagnetism and resistive switching may be observed in the same sample – both are caused by defects, such as oxygen vacancies in the case of $\text{ZrO}_2:\text{Co}_3\text{O}_4$ and $\text{HfO}_2:\text{ZrO}_2$ samples in this work. Metal oxide ferromagnetism will be discussed in the next chapter. But ferroelectricity scarcely coincides with the former properties, since defects in a material induce leakage and make the observation of ferroelectricity hard, because even if present, ferroelectricity is overwhelmed by leakage.

Ferromagnetic Properties

In the case of very thin films with thickness values of less than 100 nm, as is the case in this work, the traditional explanation with magnetic domains is not adequate, because magnetic domain sizes usually measure in the micrometer scale [29].

Ferromagnetism in such nanomaterials has been proposed to arise from various defects, for example oxygen vacancies [73], cation vacancies [74], cation interstitials [75], etc. Which defect is responsible for ferromagnetism in a material, is not easily determined and results are not unambiguous. Several authors have come to the conclusion that ferromagnetism in zirconia is induced by oxygen vacancies [18, 76] and in hafnia some conclude the reason to be oxygen vacancies [77–78], but it has also found to be induced by Hf vacancies [31].

All reports known to author nevertheless suggest that room temperature ferromagnetism in thin oxide films is caused by some defects and in the samples under study in this work almost all samples were ferromagnetic, which is in line with other observed properties, such as samples being electrically leaky and exhibit resistive switching characteristics, which are also induced by defects. Most of the samples in papers I–III were found to be soft ferromagnetics with a clearly visible saturation magnetization, highest values were around $5 \cdot 10^{-6}$ emu ($5 \cdot 10^{-9}$ A·m²), an example of which is in figure 7 [II]. For the sample on figure 7, coercive field value is 50 Oe (~ 4000 A/m) [II], which was again typical for many samples studied in papers I–IV. $\text{ZrO}_2\text{--Fe}_2\text{O}_3$ films with the highest saturation

magnetization values were also around $5 \cdot 10^{-6}$ emu ($5 \cdot 10^{-9}$ A·m²) [I], very similar to that measured by Sangalli *et al* [79].

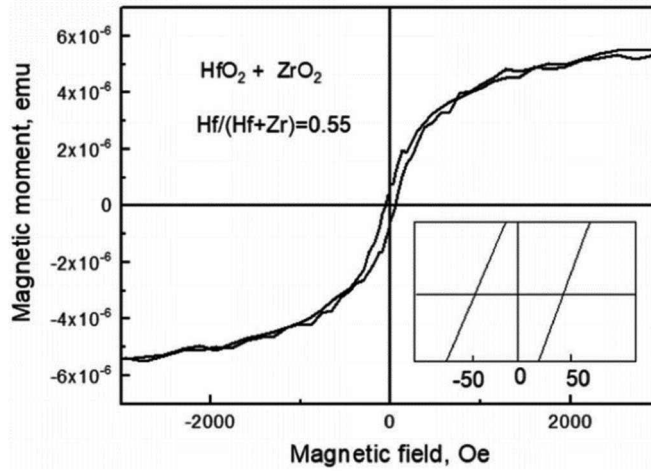


Figure 7. Ferromagnetic hysteresis curve of the same sample, for which the polarization charge graph was depicted in Fig. 5. Inset is the magnification around the origin of axes to show the coercive field value [II].

It can also be noted that as well as in the underlying papers for this thesis [I–III] and literature [18], the magnetization of ZrO₂ and samples containing ZrO₂ is correlated with the metastable tetragonal and cubic phases of ZrO₂, which are stabilized in the samples. These metastable phases are stabilized at room temperature, according to several authors, because of oxygen vacancies [18, 26, 73].

CONCLUSION

The main goal at the start of the PhD studies was to fabricate a multiferroic ultrathin film using atomic layer deposition. Method of fabrication was chosen such, because this is the method actually used in modern nanoelectronics to fabricate ultrathin films, and the only method which can provide conformal films over a large substrate area and at the same time provide thickness control at the nanometer level. It was known beforehand, from literature, that a material possessing ferromagnetic and ferroelectric behavior in the same sample in the same phase will be a difficult task. This phenomenon has been observed in bulk materials and/or at very low temperatures, but not in thin films and at room temperature. Achievement and observation of such behaviors in thin films and at temperatures actually exceeding room temperature are both necessary, if one wishes to consider an actual application in nano-electronics, such as a memory device or sensors.

ZrO₂ is a relatively simple chemical compound, known as a material, which can conveniently be grown by atomic layer deposition, and in which metastable phases can easily be stabilized. In various ZrO₂-based thin films, it was shown, in the present study, that some films demonstrated ferromagnetic hysteresis, some exhibited behavior resembling ferroelectric behavior, and some films were confirmed to work in the resistive switching regime. In one particular case, ferromagnetic and ferroelectric behavior were observed in the same material sample – a nanolaminate with 10 nm of HfO₂ and 8 nm of ZrO₂ on top of the HfO₂.

It was concluded that although one cannot speak of ferromagnetism in the traditional sense in thin metal oxide films, in certain cases ferromagnetism may still arise due to the defects in a material, such as oxygen vacancies. Although these defects make the detection of ferroelectricity harder, a reasonable trade-off can be found between defect densities sufficient for inducing ferromagnetism, but low enough to allow implications of ferroelectricity. The author believes that such a case was found in the paper II, where a defective material, which was found to behave like a ferromagnetic material in all cases, namely ZrO₂, was mixed with a less defective material, HfO₂, known already in accord with literature to be ferroelectric in some cases. Measurement results for this sample revealed ferromagnetic hysteresis and some contribution from ferroelectric hysteresis in the polarization charge *versus* applied field curves.

Resistive switching characteristics were also measured and the samples of ZrO₂:Co₃O₄ exhibited clear resistive switching behavior, resistance values for low and high states differing at most by 35 times. The resistive switching effect was also measured in some HfO₂:ZrO₂ films, making this mixture a potential candidate for the manifestation of all three studied memory effects: ferromagnetism, ferroelectricity and resistive switching.

Before the project, the author also had the hypothesis that ferromagnetism could be induced or enhanced in the samples by introducing transition metal cations, such as Fe or Co, in the samples, an opinion derived from classical

description of ferromagnetism. This was found not to be the case, as two out of three (Fe, Co, Ni) traditionally ferromagnetic metals were not found to promote ferromagnetism, when the films were deposited in oxidizing conditions. In order to establish conditions allowing one to maximize the primary parameters of magnetic characteristics of the metal oxide based multiferroics, that is saturation magnetization and coercivity, parametrization of the deposition process should be provided in detail. The optimization of the film growth in terms of screening constituent oxide cycle ratios and related effects to the crystal growth has to be provided, together with foundation of the appropriate phase composition. Possible need for post-deposition heat-treatments has to be considered and examined. Experiments devoted to the achievement of homogeneous and sufficiently dense and ordered materials layers should be continued. Well tunable deposition process might produce a) dielectric metal oxide initially in insulating state, still sufficiently defective to allow induction of current filaments enabling resistive switching, b) insulating oxide layers crystallized in an appropriate non-centrosymmetric phase, allowing ferroelectric-like behavior, and/or c) metastable oxide or doped multilayered oxide enabling the appearance of nonlinearly saturative and hysteretic magnetization.

Finally, coupling effects between magnetic and electric responses of a material were not studied yet. A multiferroic material should exhibit such coupling, if a novel data storage device is to be based on magnetoelectric effects.

SUMMARY IN ESTONIAN

Aatomkihtsadestatud tsirkooniumipõhiste nanolaminaatide ja segukilede magnetilised, elektrilised ja struktuursed omadused

Käesolevas töös kasutati aatomkihtsadestamise meetodit, eesmärgiga valmistada multiferroidne õhuke kile. Meetodi valiku põhjenduseks on asjaolu, et aatomkihtsadestamine on ennast tõestanud, kui üks sobivamaid viise üliõhukeste tahkis-kihtide valmistamiseks ühtlase paksuse ja koostisega üle suure pinna. Kirjandusallikate põhjal oli teada, et materjali valmistamine, mis oleks üheaegselt nii ferromagnetiline kui ka ferroelektriline, ei ole lihtne ülesanne. Nimetatud nähtusi on tuvastatud ühe materjali samas faasis ainult ülimaldatel temperatuuridel ja/või suurtes materjalitükkides. Autorile teadaolevalt ei ole nii magnet- kui ka elektriväljas polariseeritavat materjali suudetud valmistada õhukese materjalikihina ning toimivana ka toatemperatuuril või kõrgemal. Mõlemad nimetatud tingimused on kindlasti tarvilikud, et rääkida võimalikest praktilistest rakendustest.

ZrO₂ on lihtsa keemilise koostisega ühend, mida on võimalik aatomkihtsadestada ning stabiliseerida metastabiilsesse faasi. Erinevates ZrO₂ sisaldavates kiledes demonstreeriti osa kilede puhul ferromagnetilist hüstereesi, osa käitus elektriväljas ferroelektrikule sarnaselt ning osa kilesid töötas takistuslülituslikus režiimis. Ühel juhul tuvastati ferromagnetiline ja ferroelektriline polariseeritavus samas kilenäidises, täpsemalt kahekihilises struktuuris, kus aluse peal oli 10 nm HfO₂ kiht ning selle peal 8 nm ZrO₂ kiht.

Järeldati, et kuigi traditsioonilisest ferromagnetismist rääkimiseks ei ole õhukeste metalloksiidkilede puhul põhjust, siis teatud juhtudel võivad siiski defektid, nagu näiteks hapnikuvakantsid, materjali ferromagnetilist käitumist põhjustada. Kuigi defektid raskendavad ferroelektrilise polarisatsiooni mõõtmist, võib leida nõ. tasakaalupunkti piisava hulga defektide vahel, et saavutada ferromagnetiline polarisatsioon ja piisavalt vähese hulga defektide vahel, et ferroelektriline efekt ei jää veel täielikult piirpindadel tekkiva lekkevoolust tingitud polarisatsiooni varju. Autori arvates tuvastati selline olukord töös II, kus defektirohke ferromagnetiline ZrO₂ segati vähem defektse materjaliga HfO₂, mille puhul võis kirjandusele toetudes oodata ferroelektrilisust. Mõõtmistulemused kinnitasid kõnealuse kile ferromagnetilisust ning ferroelektrilise efekti panust polarisatsioonilaengusse.

ZrO₂:Co₃O₄ puhul tuvastati takistuslülituslik efekt, mille puhul madala ja kõrge takistusega olekud erinesid teineteisest 35 korda. Takistuslülitusena töötasid ka osad HfO₂:ZrO₂ segukiled, tehes kõnealusest materjalist potentsiaalse kandidaadi kõigi kolme mäluefekti – ferromagnetism, ferroelektrilisus, takistuslülitus – samaaegseks esinemiseks.

Enne projekti oli autoril hüpotees, et ferromagnetismi saab metalloksiidkiles indutseerida tuntud ferromagnetiliste metallide, nagu Fe ja Co, katioonide kilesse viimise kaudu. Selline arvamus oli tuletatud ferromagnetismi traditsioonilisest käsitlusest. See ei osutunud tõeseks, tüüpiliselt ferromagnetismiga seostatavad

üleminekumetallid ei omanud märgatavat mõju õhukeste metalloksiidide ferromagnetilisusele.

Järgmine suur samm kõnealuses valdkonnas oleks tuvastada materjalis vastasmõju ferromagnetilise ja ferroelektrilise koste vahel, mida käesolevas töös ei ole uuritud. Näiteks uudse multiferroidsusel põhineva mäluseadme valmistamise eeltingimuseks on selline vastasmõju vajalik.

ACKNOWLEDGEMENTS

I give my deepest gratitude to my supervisors, Dr. Aile Tamm, Dr. Kaupo Kukli and Dr. Aarne Kasikov, for their all-round support, from help with research, publishing articles and writing the dissertation to giving advice on the everyday hardships of a PhD student.

I am also very thankful to all my co-authors of the various publications we have published together.

Last, but definitely not least, none of my scientific work would have been possible without the continuous support of my wife, Britt, and our wonderful kids, who provide me the opportunity to work in the demanding field of science, but also sometimes give me the possibility to step out of the science world and keep my head clear.

REFERENCES

- 1) Nicola A. Hill “Why are there so few magnetic ferroelectrics?.” (2000): 6694–6709.
- 2) Kyung Min Kim, Doo Seok Jeong, and Cheol Seong Hwang. “Nanofilamentary resistive switching in binary oxide system; a review on the present status and outlook.” *Nanotechnology* 22, no. 25 (2011): 254002.
- 3) Shibing Long, Xiaojuan Lian, Carlo Cagli, Xavier Cartoixa, Riccardo Rurali, Enrique Miranda, David Jiménez, Luca Perniola, Ming Liu, and Jordi Suñé. “Quantum-size effects in hafnium-oxide resistive switching.” *Applied Physics Letters* 102, no. 18 (2013): 183505.
- 4) Enrique A. Miranda, Christian Walczyk, Christian Wenger, and Thomas Schroeder. “Model for the Resistive Switching Effect in HfO₂ MIM Structures Based on the Transmission Properties of Narrow Constrictions.” *IEEE Electron Device Letters* 31, no. 6 (2010): 609–611.
- 5) Nicola A. Hill, and Alessio Filippetti. “Why are there any magnetic ferroelectrics?.” *Journal of Magnetism and Magnetic Materials* 242 (2002): 976–979.
- 6) L. W. Martin, Y-H. Chu, and R. J. M. S. Ramesh. “Advances in the growth and characterization of magnetic, ferroelectric, and multiferroic oxide thin films.” *Materials Science and Engineering: R: Reports* 68, no. 4–6 (2010): 89–133.
- 7) Shaoqing Ren, Hongwei Qin, Jianpei Bu, Gengchang Zhu, Jihao Xie, and Jifan Hu. “Coexistence of electric field controlled ferromagnetism and resistive switching for TiO₂ film at room temperature.” *Applied Physics Letters* 107, no. 6 (2015): 062404.
- 8) Feng Pan, Shuang Gao, Chao Chen, Chen Song, and Fei Zeng. “Recent progress in resistive random access memories: materials, switching mechanisms, and performance.” *Materials Science and Engineering: R: Reports* 83 (2014): 1–59.
- 9) Deok-Hwang Kwon, Kyung Min Kim, Jae Hyuck Jang, Jong Myeong Jeon, Min Hwan Lee, Gun Hwan Kim, Xiang-Shu Li et al. “Atomic structure of conducting nanofilaments in TiO₂ resistive switching memory.” *Nature Nanotechnology* 5, no. 2 (2010): 148–153.
- 10) Doo Seok Jeong, Herbert Schroeder, Uwe Breuer, and Rainer Waser. “Characteristic electroforming behavior in Pt/TiO₂/Pt resistive switching cells depending on atmosphere.” *Journal of Applied Physics* 104, no. 12 (2008): 123716.
- 11) B. J. Choi, Doo Seok Jeong, S. K. Kim, C. Rohde, S. Choi, J. H. Oh, H. J. Kim et al. “Resistive switching mechanism of TiO₂ thin films grown by atomic-layer deposition.” *Journal of Applied Physics* 98, no. 3 (2005): 033715.
- 12) Stefan Slesazek, and Thomas Mikolajick. “Nanoscale resistive switching memory devices: a review.” *Nanotechnology* 30, no. 35 (2019): 352003.
- 13) Ting-Chang Chang, Kuan-Chang Chang, Tsung-Ming Tsai, Tian-Jian Chu, and Simon M. Sze. “Resistance random access memory.” *Materials Today* 19, no. 5 (2016): 254–264.
- 14) Ilia Valov. “Interfacial interactions and their impact on redox-based resistive switching memories (ReRAMs).” *Semiconductor Science and Technology* 32, no. 9 (2017): 093006.
- 15) Akihito Sawa. “Resistive switching in transition metal oxides.” *Materials Today* 11, no. 6 (2008): 28–36.
- 16) A. Berthelot, C. Caillat, V. Huard, S. Barnola, B. Boeck, H. Del-Puppo, N. Emonet, and F. Lalanne. “Highly reliable TiN/ZrO₂/TiN 3D stacked capacitors for 45 nm embedded DRAM technologies.” In *2006 European Solid-State Device Research Conference*, pp. 343–346. IEEE, 2006.

- 17) D-S. Kil, H-S. Song, K-J. Lee, Kwon Hong, J-H. Kim, K-S. Park, S-J. Yeom et al. "Development of new TiN/ZrO₂/Al₂O₃/ZrO₂/TiN capacitors extendable to 45nm generation DRAMs replacing HfO₂ based dielectrics." In *2006 Symposium on VLSI Technology, 2006. Digest of Technical Papers.*, pp. 38–39. IEEE, 2006.
- 18) Shuai Ning, Peng Zhan, Qian Xie, Zhengcao Li, and Zhengjun Zhang. "Room-temperature ferromagnetism in un-doped ZrO₂ thin films." *Journal of Physics D: Applied Physics* 46, no. 44 (2013): 445004.
- 19) J. Zippel, M. Lorenz, A. Setzer, M. Rothermel, D. Spemann, P. Esquinazi, M. Grundmann, G. Wagner, R. Denecke, and A. A. Timopheev. "Defect-induced magnetism in homoepitaxial manganese-stabilized zirconia thin films." *Journal of Physics D: Applied Physics* 46, no. 27 (2013): 275002.
- 20) V. G. Myagkov, L. E. Bykova, O. A. Bayukov, V. S. Zhigalov, I. A. Tambasov, S. M. Zharkov, A. A. Matsynin, and G. N. Bondarenko. "Solid state synthesis and characterization of Fe–ZrO₂ ferromagnetic nanocomposite thin films." *Journal of Alloys and Compounds* 636 (2015): 223–228.
- 21) Irina Kärkkäinen, Andrey Shkabko, Mikko Heikkilä, Marko Vehkamäki, Jaakko Niinistö, Nabeel Aslam, Paul Meuffels et al. "Impedance spectroscopy study of the unipolar and bipolar resistive switching states of atomic layer deposited polycrystalline ZrO₂ thin films." *physica status solidi (a)* 212, no. 4 (2015): 751–766.
- 22) T. S. Bösccke, J. Müller, D. Bräuhäus, U. Schröder, and U. Böttger. "Ferroelectricity in hafnium oxide thin films." *Applied Physics Letters* 99, no. 10 (2011): 102903.
- 23) Johannes Muller, Tim S. Boscke, Uwe Schroder, Stefan Mueller, Dennis Brauhäus, Ulrich Böttger, Lothar Frey, and Thomas Mikolajick. "Ferroelectricity in simple binary ZrO₂ and HfO₂." *Nano Letters* 12, no. 8 (2012): 4318–4323.
- 24) C. R. Aita, M. D. Wiggins, R. Whig, C. M. Scanlan, and M. Gajdardziska-Josifovska. "Thermodynamics of tetragonal zirconia formation in a nanolaminate film." *Journal of Applied Physics* 79, no. 2 (1996): 1176–1178.
- 25) Ronald C. Garvie, and Michael V. Swain. "Thermodynamics of the tetragonal to monoclinic phase transformation in constrained zirconia microcrystals." *Journal of Materials Science* 20, no. 4 (1985): 1193–1200.
- 26) Zhaoqi Zhan, and Hua C. Zeng. "Metastability of tetragonal ZrO₂ derived from Zr-n-propoxide-acetylacetone-water-isopropyl alcohol." *Journal of Materials Research* 13, no. 8 (1998): 2174–2183.
- 27) Xinyuan Zhao, and David Vanderbilt. "Phonons and lattice dielectric properties of zirconia." *Physical Review B* 65, no. 7 (2002): 075105.
- 28) Richard W. Johnson, Adam Hultqvist, and Stacey F. Bent. "A brief review of atomic layer deposition: from fundamentals to applications." *Materials Today* 17, no. 5 (2014): 236–246.
- 29) Nicola A. Spaldin *Magnetic materials: fundamentals and applications*. Cambridge University Press, 2010.
- 30) W. Heisenberg. "On the theory of ferromagnetism." *Z. Phys.*, 49:619, 1928
- 31) Georges Bouzerar, and Timothy Ziman. "Model for vacancy-induced d⁰ ferromagnetism in oxide compounds." *Physical Review Letters* 96, no. 20 (2006): 207602.
- 32) Céline Lichtensteiger, Matthew Dawber, and Jean-Marc Triscone. "Physics of ferroelectrics: A modern perspective." *Topics Appl. Physics*, eds. K. Rabe, CH Ahn and JM Triscone (2007): 305A338.

- 33) Ronald E. Cohen, and Henry Krakauer. "Electronic structure studies of the differences in ferroelectric behavior of BaTiO₃ and PbTiO₃." *Ferroelectrics* 136, no. 1 (1992): 65–83.
- 34) Steven M. George "Atomic layer deposition: an overview." *Chemical Reviews* 110, no. 1 (2010): 111–131.
- 35) G. V. Sveshnikova, S. I. Koltsov, and V. B. Aleskovskii. "Formation of a silica layer of predetermined thickness on silicon by the Molecular-Layering method." *Zh Prikl Khim* 43 (1970): 1150–1152.
- 36) S. I. Koltsov "Structural Changes of Silica Gel during Formation on Its Surface of Titanium Dioxide Layers." *Zhurnal Prikladnoi Khimii* 43, no. 9 (1970): 1956–+.
- 37) V. B. Aleskovsky "On chemistry and technology of solid substances." *Journal of Applied Chemistry* 47, no. 10 (1974): 2145.
- 38) Tuomo Suntola, and Jorma Antson. "Method for producing compound thin films." U.S. Patent 4,058,430, issued November 15, 1977.
- 39) Kaupo Kukli, Jaan Aarik, Aleks Aidla, Oksana Kohan, Teet Uustare, and Väino Sammelselg. "Properties of tantalum oxide thin films grown by atomic layer deposition." *Thin Solid Films* 260, no. 2 (1995): 135–142.
- 40) Arla Kytökiivi, Eeva-Liisa Lakomaa, Andrew Root, Heidi Österholm, Jean-Paul Jacobs, and Hidde H. Brongersma. "Sequential saturating reactions of ZrCl₄ and H₂O vapors in the modification of silica and γ -alumina with ZrO₂." *Langmuir* 13, no. 10 (1997): 2717–2725.
- 41) V. V. Brodskii, E. A. Rykova, A. A. Bagatur'yants, and A. A. Korkin. "Modelling of ZrO₂ deposition from ZrCl₄ and H₂O on the Si(100) surface: initial reactions and surface structures." *Computational Materials Science* 24, no. 1–2 (2002): 278–283.
- 42) Mikko Ritala, and Markku Leskelä. "Zirconium dioxide thin films deposited by ALE using zirconium tetrachloride as precursor." *Applied Surface Science* 75, no. 1–4 (1994): 333–340.
- 43) Hiroyuki Fujiwara. *Spectroscopic ellipsometry: principles and applications*. John Wiley & Sons, 2007.
- 44) G. E. Jellison Jr, and F. A. Modine. "Parameterization of the optical functions of amorphous materials in the interband region." *Applied Physics Letters* 69, no. 3 (1996): 371–373.
- 45) Bertram Eugene Warren. *X-ray Diffraction*. Courier Corporation, 1990.
- 46) Krassimir N. Stoev, and Kenji Sakurai. "Review on grazing incidence X-ray spectrometry and reflectometry." *Spectrochimica Acta Part B: Atomic Spectroscopy* 54, no. 1 (1999): 41–82.
- 47) Ron Jenkins. *X-ray fluorescence spectrometry*. Vol. 2. New York: Wiley, 1999.
- 48) Anwar Ul-Hamid. *A Beginners' Guide to Scanning Electron Microscopy*. Springer, 2018.
- 49) Simon Foner. "Review of magnetometry." *IEEE Transactions on Magnetics* 17, no. 6 (1981): 3358–3363.
- 50) Simon Foner. "Versatile and sensitive vibrating-sample magnetometer." *Review of Scientific Instruments* 30, no. 7 (1959): 548–557.
- 51) Genhua Pan. "Thin films for high-density magnetic recording." In *Handbook of Thin Films*, pp. 495–553. Academic Press, 2002.
- 52) Charles Baldwin Sawyer, and C. H. Tower. "Rochelle salt as a dielectric." *Physical Review* 35, no. 3 (1930): 269.

- 53) Sadhan Chandra Das, Aga Shahee, N. P. Lalla, and T. Shripathi. "A simple and low cost Sawyer-Tower ferro-electric loop tracer with variable frequency and compensation circuit." In *Proceedings of the 54th DAE Solid State Physics Symposium Volume*, vol. 54, no. D1, pp. 439–440. 2009.
- 54) Alex BF Martinson, Michael J. DeVries, Joseph A. Libera, Steven T. Christensen, Joseph T. Hupp, Michael J. Pellin, and Jeffrey W. Elam. "Atomic layer deposition of Fe_2O_3 using ferrocene and ozone." *The Journal of Physical Chemistry C* 115, no. 10 (2011): 4333–4339.
- 55) J. W. Elam, Z. A. Sechrist, and S. M. George. "ZnO/ Al_2O_3 nanolaminates fabricated by atomic layer deposition: growth and surface roughness measurements." *Thin Solid Films* 414, no. 1 (2002): 43–55.
- 56) Kaupo Kukli, Marianna Kemell, Joel Köykkä, Kenichiro Mizohata, Marko Vehkamäki, Mikko Ritala, and Markku Leskelä. "Atomic layer deposition of zirconium dioxide from zirconium tetrachloride and ozone." *Thin Solid Films* 589 (2015): 597–604.
- 57) Kevin J. Hughes, and James R. Engstrom. "Nucleation delay in atomic layer deposition on a thin organic layer and the role of reaction thermochemistry." *Journal of Vacuum Science & Technology A: Vacuum, Surfaces, and Films* 30, no. 1 (2012): 01A102.
- 58) Kaupo Kukli, Mikko Ritala, Jaan Aarik, Teet Uustare, and Markku Leskelä. "Influence of growth temperature on properties of zirconium dioxide films grown by atomic layer deposition." *Journal of Applied Physics* 92, no. 4 (2002): 1833–1840.
- 59) Kaupo Kukli, Katarina Forsgren, Jaan Aarik, Teet Uustare, Aleks Aidla, Antti Niskanen, Mikko Ritala, Markku Leskelä, and Anders Hårsta. "Atomic layer deposition of zirconium oxide from zirconium tetraiodide, water and hydrogen peroxide." *Journal of Crystal Growth* 231, no. 1–2 (2001): 262–272.
- 60) Jaan Aarik, Aleks Aidla, Hugo Mändar, Teet Uustare, and Väino Sammelselg. "Growth kinetics and structure formation of ZrO_2 thin films in chloride-based atomic layer deposition process." *Thin Solid Films* 408, no. 1–2 (2002): 97–103.
- 61) Yuh-Chen Lin, Felicia McGuire, and Aaron D. Franklin. "Realizing ferroelectric $\text{Hf}_{0.5}\text{Zr}_{0.5}\text{O}_2$ with elemental capping layers." *Journal of Vacuum Science & Technology B, Nanotechnology and Microelectronics: Materials, Processing, Measurement, and Phenomena* 36, no. 1 (2018): 011204.
- 62) Erik Østreng, Henrik H. Sønsteby, Timo Sajavaara, Ola Nilsen, and Helmer Fjellvåg. "Atomic layer deposition of ferroelectric LiNbO_3 ." *Journal of Materials Chemistry C* 1, no. 27 (2013): 4283–4290.
- 63) Henrik Hovde Sønsteby. "Piezo-and Ferroelectric $\text{A}^+\text{B}^{5+}\text{O}_3$ Thin Films." (2017). PhD thesis.
- 64) Marko Vehkamäki, Timo Hatanpää, Marianna Kemell, Mikko Ritala, and Markku Leskelä. "Atomic layer deposition of ferroelectric bismuth titanate $\text{Bi}_4\text{Ti}_3\text{O}_{12}$ thin films." *Chemistry of Materials* 18, no. 16 (2006): 3883–3888.
- 65) Feng Zhang, Ya-Chuan Perng, Ju H. Choi, Tao Wu, Tien-Kan Chung, Gregory P. Carman, Christopher Locke, Sylvia Thomas, Stephen E. Sadow, and Jane P. Chang. "Atomic layer deposition of $\text{Pb}(\text{Zr},\text{Ti})\text{O}_x$ on 4H-SiC for metal-ferroelectric-insulator-semiconductor diodes." *Journal of Applied Physics* 109, no. 12 (2011): 124109.
- 66) J. F. Scott "Ferroelectrics go bananas." *Journal of Physics: Condensed Matter* 20, no. 2 (2007): 021001.

- 67) Dominik Martin, Johannes Müller, Tony Schenk, Thomas M. Arruda, Amit Kumar, Evgheni Strelcov, Ekaterina Yurchuk et al. "Ferroelectricity in Si-Doped HfO₂ Revealed: A Binary Lead-Free Ferroelectric." *Advanced Materials* 26, no. 48 (2014): 8198–8202.
- 68) Stephen L. Weeks, Ashish Pal, Vijay K. Narasimhan, Karl A. Littau, and Tony Chiang. "Engineering of ferroelectric HfO₂-ZrO₂ nanolaminates." *ACS Applied Materials & Interfaces* 9, no. 15 (2017): 13440–13447.
- 69) Xiaoyong Xu, Chunxiang Xu, Jun Dai, Jingguo Hu, Fengji Li, and Sam Zhang. "Size dependence of defect-induced room temperature ferromagnetism in undoped ZnO nanoparticles." *The Journal of Physical Chemistry C* 116, no. 15 (2012): 8813–8818.
- 70) M. Khalid, M. Ziese, A. Setzer, P. Esquinazi, M. Lorenz, H. Hochmuth, M. Grundmann et al. "Defect-induced magnetic order in pure ZnO films." *Physical Review B* 80, no. 3 (2009): 035331.
- 71) Tongfei Shi, Zhenguo Xiao, Zhijun Yin, Xinhua Li, Yuqi Wang, Hongtao He, Jiannong Wang, Wenshen Yan, and Shiqiang Wei. "The role of Zn interstitials in cobalt-doped ZnO diluted magnetic semiconductors." *Applied Physics Letters* 96, no. 21 (2010): 211905.
- 72) Parmod Kumar, Vikas Sharma, Ankita Sarwa, Ashish Kumar, Rajan Goyal, K. Sachdev, S. Annapoorni, K. Asokan, and D. Kanjilal. "Understanding the origin of ferromagnetism in Er-doped ZnO system." *RSC Advances* 6, no. 92 (2016): 89242–89249.
- 73) M. Venkatesan, C. B. Fitzgerald, and J. M. D. Coey. "Unexpected magnetism in a dielectric oxide." *Nature* 430, no. 7000 (2004): 630–630.
- 74) Nguyen Hoa Hong, Nathalie Poirrot, and Joe Sakai. "Evidence for magnetism due to oxygen vacancies in Fe-doped HfO₂ thin films." *Applied Physics Letters* 89, no. 4 (2006): 042503.
- 75) Davide Sangalli, Alessio Lamperti, Elena Cianci, Roberta Ciprian, Michele Perego, and Alberto Debernardi. "Role of oxygen vacancies on the structure and density of states of iron-doped zirconia." *Physical Review B* 87, no. 8 (2013): 085206.

PUBLICATIONS

CURRICULUM VITAE

Name Kristjan Kalam
Date of birth 4.05.1989
E-mail kristjan.kalam@ut.ee

Institution and position

01.05.2018–
30.04.2020 University of Tartu, Faculty of Science and Technology,
Institute of Physics, Junior Research Fellow in Material Science
(0,40)
01.09.2017–... Estonian Aviation Academy, lecturer
2016–... University of Tartu, Faculty of Science and Technology,
Institute of Physics, Laboratory of of Thin-Film Technology,
PhD student (1,00)

Education

2016–... University of Tartu, Doctor of Philosophy, Materials Science
2014–2016 University of Tartu, physics, M.Sc (cum laude)
2011–2014 University of Tartu, physics, B.Sc
1996–2008 Tallinn Secondary Science School

Academic degrees

Kristjan Kalam, Master's Degree, 2016, (supervisor) Aarne Kasikov,
Aatomkihtsadestatud ternaarsete oksiidide ellipsomeetria (Ellipsometry of
ternary oxides grown by atomic layer deposition), University of Tartu, Faculty
of Science and Technology (old), Institute of Physics, University of Tartu.
Kristjan Kalam, Phd student, (supervisors) Aile Tamm; Kaupo Kukli; Aarne
Kasikov, Structural and magnetoelectric analysis of multifunctional
nanolaminates and solid solutions grown by atomic layer deposition,
University of Tartu, Faculty of Science and Technology, Institute of Physics.

Projects in progress

TK134 “Kontrollitud korrastatus kvant- ja nanomaterjalides (1.01.2016–
1.03.2023)”, Tamm, Aile, Tartu Ülikool, Loodus- ja täppisteaduste valdkond,
Füüsika instituut.
PRG4 “Tugevalt frustrereitud kvantmagnetite adapteeruvad olekud (ENIQMA)
(1.01.2018–31.12.2022)”, Raivo Stern, Keemilise ja Bioloogilise Füüsika
Instituut.
TK141 “Uudsed materjalid ja kõrgtehnoloogilised seadmed energia salvestamise
ja muundamise süsteemidele (1.01.2016–1.03.2023)”, Enn Lust, Tartu Üli-
kool, Loodus- ja täppisteaduste valdkond.

Publications

Number of publications: 9
1 oral and 3 poster presentations at international conferences

ELULOOKIRJELDUS

Nimi Kristjan Kalam
Sünniaeg 4.05.1989
E-post kristjan.kalam@ut.ee

Töökohad ja ametid

01.05.2018–
30.04.2020 Tartu Ülikool, Loodus- ja täppisteaduste valdkond, füüsika instituut, materjaliteaduse nooremteadur (0,40)
01.09.2017–... Eesti Lennuakadeemia, lektor
2016–... Tartu Ülikool, Loodus- ja tehnoloogiateaduskond, Tartu Ülikooli Füüsika Instituut, Kiletehnoloogia labor, doktorant (1,00)

Haridustee

2016–... Tartu Ülikool, doktoriõpe, materjaliteadus
2014–2016 Tartu Ülikool, magistriõpe, füüsika (cum laude)
2011–2014 Tartu Ülikool, bakalaureuseõpe, füüsika
1996–2008 Tallinna Reaalkool, Keskkharidus

Teaduskraadid

Kristjan Kalam, magistrikraad, 2016, (juh) Aarne Kasikov, Aatomkihtsadestatud ternaarsete oksiidide ellipsomeetria, Tartu Ülikool.
Kristjan Kalam, doktorant, (juh) Aile Tamm; Kaupo Kukli; Aarne Kasikov, Structural and magnetoelectric analysis of multifunctional nanolaminates and solid solutions grown by atomic layer deposition, Tartu Ülikool.

Jooksvad projektid

TK134 “Kontrollitud korrastatus kvant- ja nanomaterjalides (1.01.2016–1.03.2023)”, Tamm, Aile, Tartu Ülikool, Loodus- ja täppisteaduste valdkond, Füüsika instituut.
PRG4 “Tugevalt frustreritud kvantmagnetite adapteeruvad olekud (ENIQMA) (1.01.2018–31.12.2022)”, Raivo Stern, Keemilise ja Bioloogilise Füüsika Instituut.
TK141 “Uudsed materjalid ja kõrgtehnoloogilised seadmed energia salvestamise ja muundamise süsteemidele (1.01.2016–1.03.2023)”, Enn Lust, Tartu Ülikool, Loodus- ja täppisteaduste valdkond.

Publikatsioonid

Publikatsioonide üldarv: 9
3 posterettekannet ja 1 suuline ettekanne rahvusvahelistel konverentsidel.

DISSERTATIONES SCIENTIAE MATERIALIS UNIVERSITATIS TARTUENSIS

1. **Martin Järvekülg.** Tubular microstructures by Hf-, Zr- and Ti-butoxide gel sheet rolling. Tartu, 2011, 112 p.
2. **Sergei Vlassov.** Investigation of nanoscale interactions and mechanical properties of nanostructures using quartz tuning fork based real-time measurements. Tartu, 2011, 171 p.
3. **Margus Kodu.** Pulsed Laser Deposition of Magnesium Oxide and Barium Ternary Oxides for Plasma Display Protective Layers. Tartu, 2011, 89 p.
4. **Rainer Pärna.** Surface studies of some oxide films. Tartu, 2011, 129 p.
5. **Jevgeni Šulga.** Self-assembly and interaction of nanostructures. Tartu, 2011, 114 p.
6. **Wojciech Kuznik.** Quantum-chemical computer simulations of the linear and non-linear optical properties of pyrazoloquinoline and dicyanopyrazine derivatives. Tartu, 2012, 89 p.
7. **Leonid Dorogin.** Structural and tribological properties of zero- and one-dimensional nanocrystals. Tartu, 2012, 193 p.
8. **Viljar Palmre.** Fabrication and characterization of microporous carbon-based electroactive polymer actuators. Tartu, 2012, 99 p.
9. **Madis Paalo.** Synthesis of CNT-metal oxide nanocomposites: sol-gel process, rheology, structural and functional properties. Tartu, 2014, 175 p.
10. **Raul Välbe.** Development of ionic liquid composites by sol-gel method for elaboration of industrial nano- and microstructures. Tartu, 2014, 97 p.
11. **Urmas Joost.** Impurity and preparation dependent properties of titania thin films. Tartu, 2014, 155 p.
12. **Madis Umalas.** Application of sol-gel technology for production of ceramic nanocomposites and functional coatings. Tartu, 2015, 136 p.
13. **Elena Samsonova.** Energy transfer probe as a tool to study morphological and structural origins of fluorescence quenching in rare-earth doped nanophosphors. Tartu, 2015, 114 p.
14. **Jay Mondal.** Novel Corrosion Protective Nanostructured Composite Coatings. Tartu, 2016, 104 p.
15. **Kathriin Utt.** Metal oxide mesostructures for optical applications. Tartu, 2016, 88 p.
16. **Kaido Siimon.** Electrospun gelatin cross-linked by glucose. Tartu, 2016, 84 p.
17. **Marko Part.** Combined three-dimensional sol-gel structures and atomic layer deposited thin films. Tartu, 2017, 162 p.
18. **Pejman Rasti.** Analysis of Remote Sensing Image Super Resolution using Fluid Lenses. Tartu, 2017, 188 p.
19. **Ivo Romet.** Recombination luminescence of doped borates: origin and application prospects in dosimetry. Tartu, 2017, 111 p.

20. **Vladimir I. Kondratiev.** Processing and characterization of transparent electrode materials. Tartu, 2017, 111 p.
21. **Taivo Jõgiaas.** Mechanical properties of atomic layer deposited thin films and nanocomposites. Tartu, 2017, 125 p.
22. **Lauri Aarik.** Atomic layer deposition and characterization of thin oxide films for application in protective coatings. Tartu, 2017, 180 p.
23. **Triin Kangur.** Preparation and functional properties of stochastic micro-structured sol-gel silica materials. Tartu, 2018, 96 p.
24. **Marta Berholts.** Fragmentation of ionic and hydrogen-bonded molecules induced by synchrotron radiation. Tartu, 2018, 126 p.
25. **Priit Priimägi.** Development and optimization of 3D-microbatteries. Tartu, 2018, 118 p.
26. **Siim Hödemann.** Residual stress determination in chemically strengthened and thermally tempered glass plates using scattered light method. Tartu, 2019, 146 p.
27. **Jekaterina Kozlova.** Complex characterization of graphene structures on nanometer level. Tartu, 2019, 206 p.